Effect of Piezo Sensor Design on EM Impedance-Based Process Monitoring and Guided Wave Based Structural Health Monitoring for Cryogenic Composite Propellant Tanks

MICHAEL SCHEERER, ZOLTAN SIMON
and MICHAEL MARISCHLER

ABSTRACT

Within this work, different sensor designs were analyzed with respect to EM impedance-based process monitoring and guided wave based structural health monitoring. Therefore, fully coupled piezo-structural harmonic and transient FE simulation are performed on the different sensor designs to assess the change of the EM impedance before and after curing and guided wave propagation and defect interaction in composite plates. The simulation results are experimentally validated by EM impedance measurements before and during curing and the measurement of the response of the bonded sensors during guided wave propagation and defect interaction on composite plates.

INTRODUCTION

Within the last years, the authors developed a hybrid multifunctional piezo / temperature sensor concept for process and structural health monitoring of composite parts made by resin transfer molding. The developed sensor consists of a piezo disc of 15 mm in diameter and 2 mm in thickness. The upper electrode is connected to a Pt100 temperature sensor using a shunt resistor, which is soldered to a circuit board that also hosts the connector. The piezo – Pt100 assembly is embedded in an epoxy housing (diameter of 20 mm and height of 10 mm). For process monitoring the impedance of the Piezo is measured during resin infusion and curing via the voltage response of the PT100 temperature sensor were the series connection of the PT100 – Piezo was actuated by frequency swept chirp signal [1, 2]. After demolding of the part, the co-cured sensor is used for either guided wave or Acoustic Emission based structural health monitoring, where the temperature information of the PT 100 sensor is used for temperature compensation. The sensor performance and the overall monitoring concept were validated on different composite parts like flat plates, a PAX door edge-member, and a hollow composite aircraft part. [3, 4, 5, 6]. The bulky design of the sensor is driven by the boundary condition of the RTM process including integration and demolding.

In recent years, the development of (reusable) cryogenic propellent tanks made of CFRP for space and aeronautic application are continuously growing. These composite

Michael Scheerer, Zoltan Simon, Michael Marischler, Aerospace & Advanced Composites GmbH, Viktor Kaplan Straße 2, Wiener Neustadt 2700, Austria

structures must be able to withstand extreme conditions without compromising safety and functionality and therefore structural health monitoring is beneficial. Typical production techniques for such tanks are filament or tape winding where pre-impregnated carbon fibers or tapes are winded around a Mandrel [7]. As such the process differs significantly from production via resin transfer molding. The aim of the presented work is to analyze different designs of the above-mentioned sensor concept to be used in cryogenic propellent composite tanks depending on the integration technique. Sensor integration can be done on the inner or outer surface of the cryogenic composite propellant tank or by embedding it in the composite structure. In the case of integration inside the tank the same sensor design might be used where the sensors are placed on predefined locations in the Mandrel like the placement in the mold in RTM processes. Such integration process has already been successfully proven on a hollow composite part using a 4-part separable inner mold like placement in a separable mandrel [6]. In the case of integration on the outer surface or embedding, new sensor designs of the sensor are needed. To assess the sensor design, three different available sensor designs were investigated with respect to EM impedance-based process monitoring and guided wave based structural health monitoring.

EXPERIMENTAL SETUP

CFRP Plates and Sensors

Two available foil type sensors – single smart layer® sensor from Acellent, DurAct P-876.SP1 sensor from PI – and AAC´s cylindric sensor were investigated. Therefore 5 sensors of each type were glued on three nominal identical 500 x 500 x 2 mm CFRP plates of $[0/90]_s$ layup using a 2K epoxy adhesive. Before and during glueing the impedance spectra of one of each type of sensor was measured to assess the influence of curing. For guided wave measurements the lower, left sensor (act) was used as actuator and sensors 1, 2, 3 and 4 were used to measure the response of propagating guided waves as shown in figure 1. The distance between the act and sensor 1 and sensor 3 as well as the distance between sensor 1 and 2 and sensor 3 and 4 is 100 mm. Sensors 1 and 2 are orientated in 0° and sensors 3 and 4 at 45° to the 0° fiber direction.

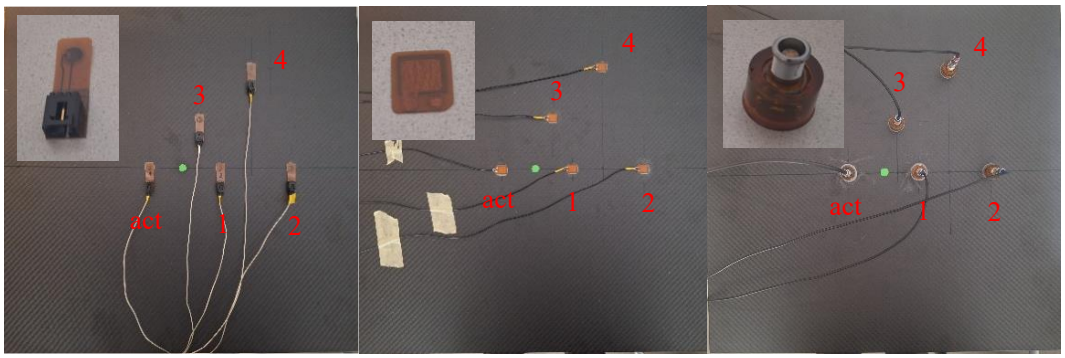

Figure 1. CFRP plates with glued smart layer® (left), DurAct (middle) and AAC (right) sensors, green plasticine – simulated damage between act and sensor 1 and enlarged image of the three sensors.

Measurement Hardware

For the measurement of the impedance of the sensors before and after glueing a LCR meter type 7600 from Quadtech was used in a frequency range of 50kHz to 500 kHz. The system for guided wave generation and measurement consists of two 4 channel acoustic emission cards (type PCI-DISP-4 from PAC) and an arbitrary waveform generator card (type: ARB-1410 from PAC) used to generate 3-sin burst signals between 40kH and 250kHz in 10 kHz steps. All acquired signals were amplified with preamplifiers of type PAC WD with an amplification of 40dB [6].

SIMULATION APPROACH

For the determination of the impedance fully coupled piezo-structural harmonic FE simulations with ANSYS in a frequency range of 50 kHz to 500 kHz were performed on an unbonded and bonded sensor of the three types of sensors. For bonding a 100x100 mm portion of the CFRP plate was taken. Guided wave propagation was assessed using fully coupled piezo-structural transient FE simulations with ANSYS of the three configurations shown in figure 1. Simulated damages placed between act and sensor 1 are approximated by cylinders made of highly damping plasticine with a diameter of 10 mm and a height of 1mm. For actuation 3-sin-burst signals at 40kHz and 100 kHz with a maximum voltage of 35V were used. The average element size in all models was 1.5 mm. Table I and Table II summarizes the used material properties. The used piezo material was PIC-255 from PI (smart layer®: d=6.3mm, t=0.1 mm / DurAct 10x10x0.2 mm / AAC: d=15mm, t=2 mm). The foils of smart layer® and DurAct sensors are made of polyimide. The AAC sensor was composed of the piezo, FR4 for the Platine containing the PT100 sensor, a connector made of bronze and polyimide, and the epoxy housing. All sensors were glued with a 2K structural adhesive of a nominal thickness of 0.1 mm. The stiffness tensor of the CFRP materials was calculated by a unit cell model.

TABLE I. MATERIAL DATA OF PIC-255 (PIEZO)

Stiffness tensor [GPa]						**Coupling coefficients [N/C]**			**Relative permittivity**	**Damping (stiffness)**
123	76.7	70.3	0	0	0	0	0	-7.15	930	$3x10^{-9}$
	123	70.3	0	0	0	0	0	-7.15	930	
		97.1	0	0	0	0	0	13.7	857	
			22.6	0	0	0	0	0		
				22.6	0	0	11.9	0		
					23.2	11.9	0	0		

TABLE II. MATERIAL DATA OF EPOXY, ADHESIVE, POLYIMIDE, BRONZE, CFRP AND CFRP [0/90]

EPOXY HOUSING		**ADHESIVE**	**CFRP [0/90]**		**FR4**
E [GPa]	2.9	3.6	E_{xx}, E_{yy} [GPa]	73, 69	21.4
ν	0.35	0.35	E_z [GPa]	9	8.1
Damping stiffness	$1x10^{-7}$	$5x10^{-7}$	G_{xy} [GPa]	4.5	3.23
POLYIMIDE		**BRONZE**	G_{yz} G_{xz} [GPa]	3.6	2.92
E [GPa]	3.5	108	ν_{xy}	0.05	0.011
ν	0.35	0.35	ν_{yz}, ν_{xz},	0.3	0.29
Damping stiffness	$1x10^{-7}$	$1x10^{-8}$	Damping stiffness	$5x10^{-8}$	$5x10^{-8}$

RESULTS

Change of Impedance due to Adhesive Curing

Figure 2 shows typical simulated resonance pattern of the bonded sensors at 100 kHz and the simulated and measured impedance "Z" as function of the frequency for the smart layer®, DurAct and AAC sensor. The measured impedances are displayed during the time of curing to illustrate the evaluation of the resonance behavior. For both the smart layer® and the DurAct sensor the prediction of the simulation fit well with the measurements of the free sensor and the fully bonded sensor at the end of curing where the resonance peaks at around 352 kHz and 171 kHz of the free sensor nearly disappear after full curing of the adhesive. For the AAC sensor the simulation shows more side resonances compared to the measurement. The reason for that can be found in uncertainties of the damping properties of the different components of the sensor. In general, the prediction of the main resonances and the influence of the curing are good. In contrast to the other sensors, a resonance peak after full curing of the adhesive is still present. The resonance peak is shifted by around 15kHz from 142 kHz to 157 kHz from unbonded to the bonded sensors. The reason for such behaviour can be found in the much thicker and subsequent stiffer piezo disc. For all sensor types, the evolution of the impedance spectra shows a clear shift of the resonance to higher frequencies with a clear increase of damping – reduction of the impedance at the resonance.

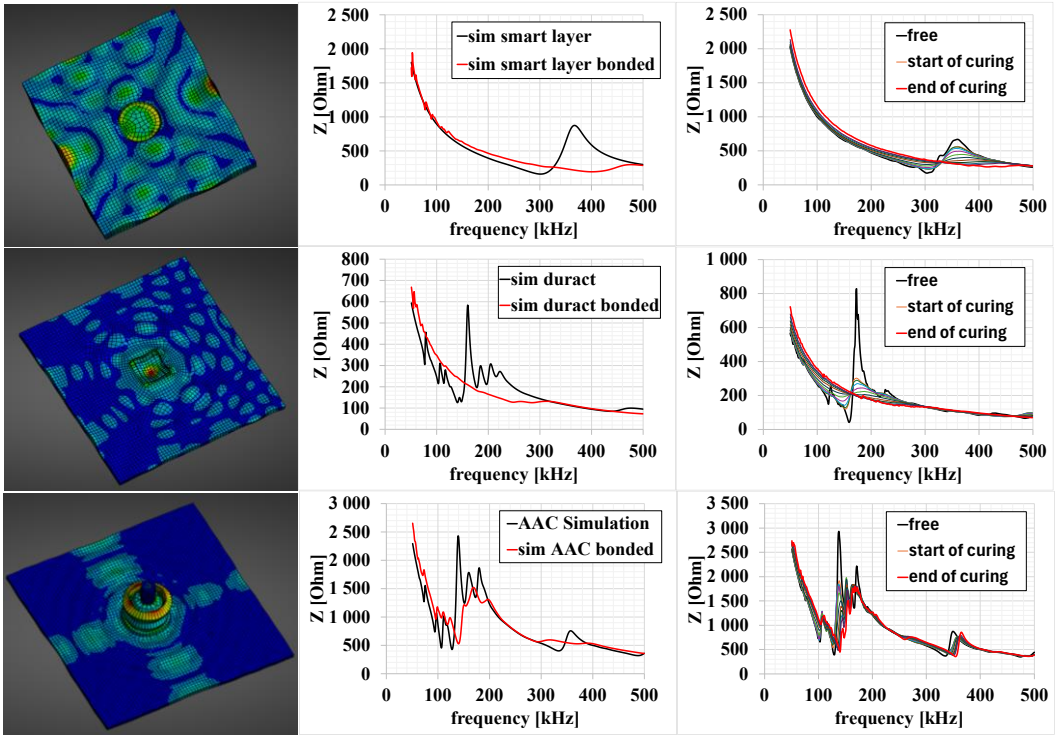

Figure 2. Typical simulated resonance pattern of the bonded sensors (left), simulated impedance Z as function of the frequency (middle) and measured impedance Z as function of the frequency (right) for the smart layer® (top), DurAct (middle) and AAC sensor (bottom).

Guided Wave Propagation

Figure 3 shows the radial (center of coordinate system at the position of act) in-plane displacement distribution over the plates with the three types of sensors at the time when the quicker S_0 mode arrives at sensor 2, the in-plane radial and out of plane displacement in the middle of the CFRP plate below the center of sensor 1 and voltage at sensor 1 and the comparison of the simulated and measured voltage response of sensors 1 and 2 for an actuation frequency of 100 kHz. Both the quicker anisotropic propagating S_0 mode and the much slower more isotropic A_0 mode can be identified in all three configurations. The larger the piezo sensor, the more dominant is the S_0 mode compared to the A_0 mode at this frequency (tuning effect) and the larger is the influence on the propagating guided wave modes. In case of the AAC sensor 1 this effect leads to S_0 to A_0 mode converted reflected wave modes. For the smart layer®

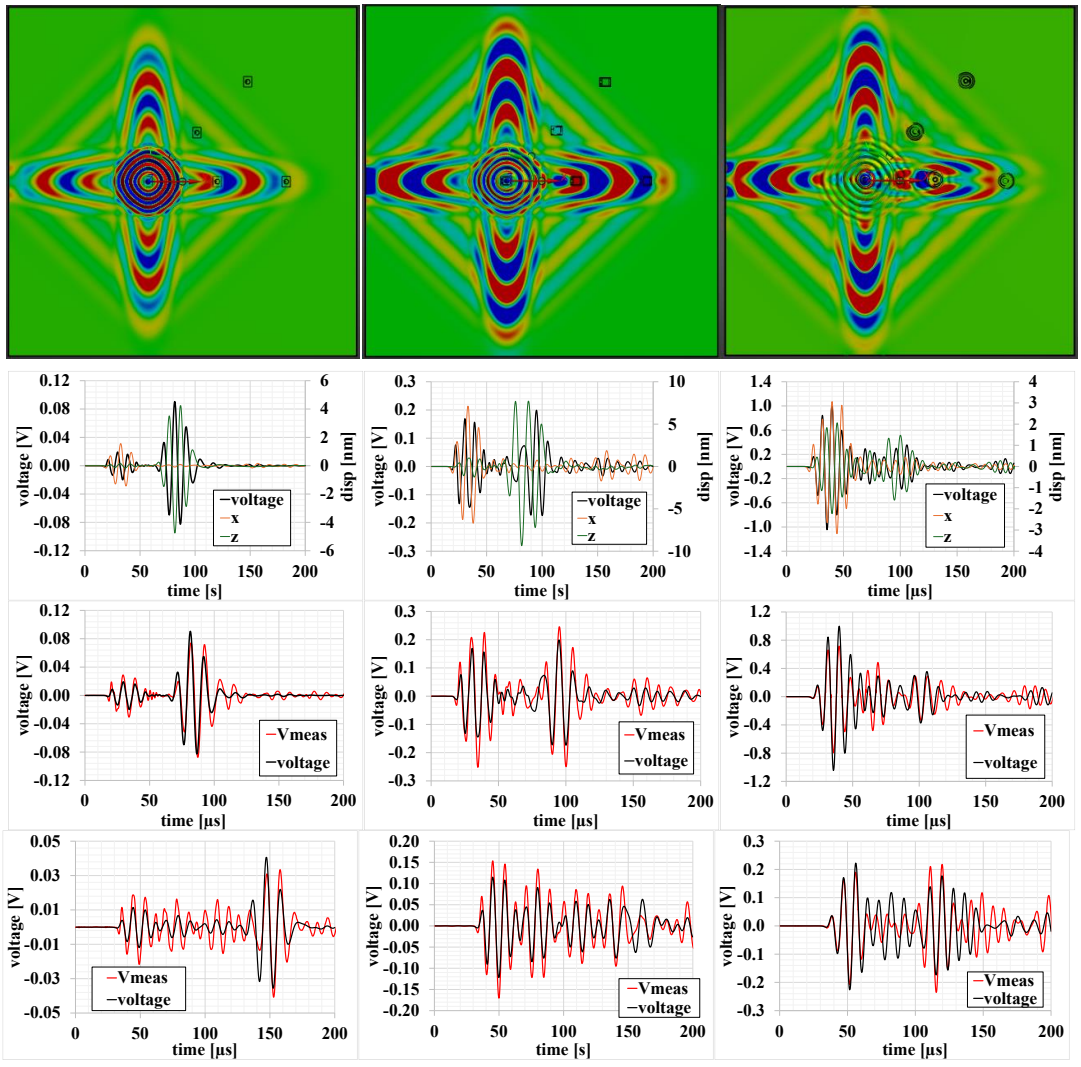

Figure 3. Radial in plane displacement distribution over the different plates with the three type of sensors (smart layer® – left, DurAct – middle, AAC – right) at a time when the quicker S0 mode arrives at sensor 2 (top), the radial in-plane and out of plane displacement and voltage at sensor 1 (2nd row) and the comparison of the measured and simulated voltage response of sensors 1 (3rd row) and sensor 2 (bottom) for an actuation frequency of 100 kHz.

sensor and the DurAct sensor the much larger in-plane deformations at around 30 µs correspond to the S_0 mode and the much larger out of plane deformation at around 80 µs correspond to the A_0 mode. For the AAC sensor with its much thicker piezo disc this effect was much less pronounced and the in-plane and out of plane components at the arrival time of the S_0 mode at sensor 1 are similar. The arrival times correspond well with the expected group velocities of 6550 m/s for the S_0 and 1500 m/s for the A_0 mode at 100 kHz in the 0° direction of the CFRP plate determined with DC calculator from DLR. The dominant in plane displacement caused by the S_0 mode at the position of sensors 1 was slightly shifted compared to the measured voltage of the piezo, which is caused by the averaging of the voltage over the piezo electrode. For all three sensors the S_0 (1^{st} wave package) and for the smart layer® and the DurAct sensor A_0 mode (2^{nd} wave package) can be clearly identified. For the AAC sensor the interaction of the back reflected S_0 to A_0 mode converted wave, which interacts with forward propagating A_0 mode makes the identification of the A_0 mode more difficult. The correlation of the measured voltage signals for the different sensors with the simulation results beside the amplitude is very good. The deviation in the amplitudes arises from different damping properties of the S_0 and A_0 mode, which cannot be modeled in ANSYS that only allows material dependent damping. The signals at sensors 2 already reflect the complexity of the wave field that arise from reflections and mode conversions of the S_0 mode on other sensors and boundaries.

Effect of Simulated Defect

The influence of the sensor design on damage detection was assessed by a simulated defect using a cylindrical batch of high damping plasticine of 10 mm in diameter and 1 mm height placed between act and sensor 1 (defect 1 – D1 / see position of defect 1 on figure 1) and act and sensor 3 (defect 2 – D2). Actuation frequencies of 40 kHz (dominant A_0 mode) and 100 kHz were used in the simulation and the experiment. Figure 4 shows the simulated and measured baseline (BL), damage (D) and residual voltage (difference between D and BL) of sensor 1 at 40kHz and 100kHz for the three sensor types. The simulation results show that all three sensors show similar residual signals at 40 kHz at the arrival time of the dominant A_0 mode at sensor 1. At 100 kHz the highest residual voltage also at the arrival time of the A_0 mode was observed for the smart layer® sensor followed by the DurAct sensor, whereas only small residuals were predicted for the AAC sensor at the arrival time of S_0 and A_0 mode. As the simulated defect is an unsymmetric highly damping added mass, it is expected that such simulated defect will mainly influence the out of plane movements of the guided waves. Therefore, mainly the A_0 mode is influenced in the case of the smart layer® and DurAct sensor. In case of the AAC sensor also at the arrival of the S_0 mode out of plane movements are present, which are influenced by the defect. The measured results are well in line with the predictions from the simulation showing slightly higher residual signals compared to the simulations. Figure 5 summarizes the capability for the detection of the specific damage of the different sensors based on a damage index DI calculated for each of the 4 sensors for the three sensor types at 40 kHz and 100kHz. The damage index DI was calculated as root mean square deviation in the time window 0 to 300 µs to capture both the A_0 and the S_0 mode. As expected,

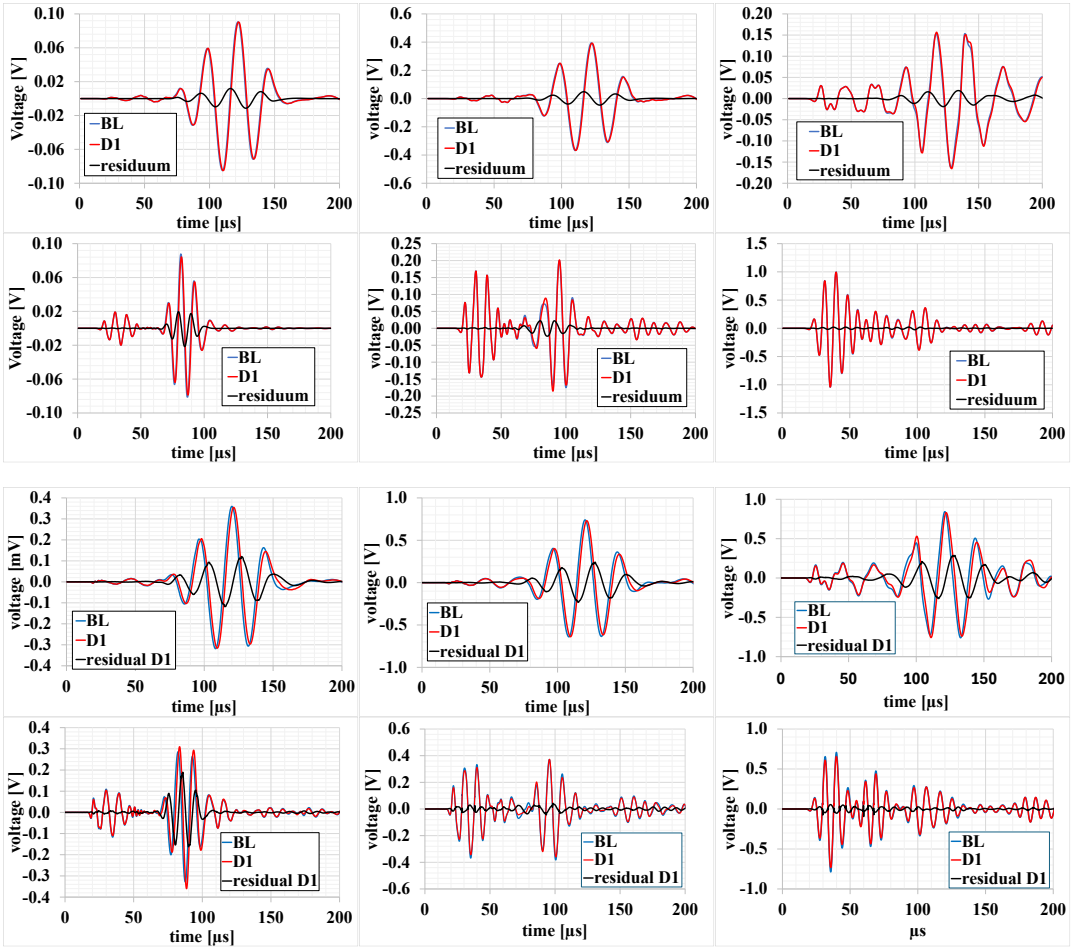

Figure 4. Simulated (row 1 and 2) and measured (row 3 and 4) baseline (BL), damage (D) and residual voltage (difference between D and BL) of sensor 1 at 40kHz (row 1 and 3) and 100kHz (row 2 and 4) for the smart layer® (left), DurAct (middle) and AAC sensor (right).

the DI was highest for the direct path's "act" to S1 and S2 for D1 and act to S3 and S4 for D2. At 40 kHz the DI for all three types of sensors is similar, where the DI is smaller for damage 2 oriented in 45° direction relative to the fiber direction. At 100 kHz the highest DI and subsequent best suitability for damage detection was found for the smart layer® sensor followed by the DurAct sensor whereas only a small DI was observed for the AAC sensor.

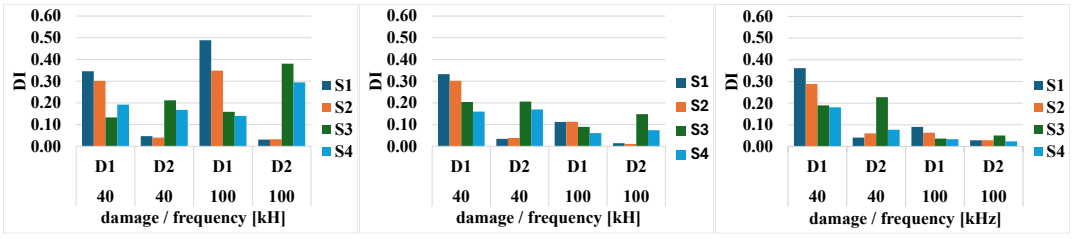

Figure 5. Damage index for the 4 sensors for damage 1 (D1) and damage 2 (D2) for 40kHz and 100kHz actuation for the smart layer® (left), DurAct (middle) and AAC sensor (right).

CONCLUSION

Three different sensors – smart layer® sensor, DurAct sensor and AAC´s cylindrical piezo temperature sensor – were theoretically and experimentally analyzed with respect to its ability for impedance-based process monitoring and guided wave based structural health monitoring of composite structures. The applied fully coupled piezo-structural harmonic and fully coupled piezo-structural transient FE simulation are in good agreement with the measured impedance curves and the voltage response of the different sensors caused by the guided waves. Especially the simulation results of the wave propagation properties are important for the interpretation of the voltage response of the different sensors. The change of the impedance at the 1st radial resonance of all three sensors can be used to monitor the curing process. The damage detection capability of the simulated defect depends on sensor design, especially on the size of the used piezo, and the actuation frequency.

AKNOWLEDGEMENT

The presented work has been funded by the Austrian Promotion Agency within the ASAP project Life Monitoring of Composite Space Structures “LiMoCoSS”.

REFERENCES

1. B. Xu, V. Giurgiutiu, “A Low-Cost and Field Portable Electromechanical (E/M) Impedance Analyzer for Active Structural Health Monitoring”, Proc. of the 5th. Int. Workshop on Structural Health Monitoring, September 15.-17.09.2005, Stanford, USA
2. V. Giurgiutiu “Structural Health Monitoring with Piezoelectric waver active sensors”. Academic Press, 2008
3. M. Scheerer, Z. Simon, M. Marischler, T. Roser, B. Rittenschober, „Validation testing of an integrated process and structural health monitoring system based on piezoelectric sensors on a PAX door edgemember made by RTM”, Proc. of the 8th. EWSHM, 05.-08.07.2016, Bilboa, Spain
4. M. Scheerer, Z. Simon, M. Marischler, B. Rittenschober, „Validation of a multifunctional hybrid piezo / temperature sensor for process and structural health monitoring of CFRP structures”, Proc. of the 9th EWSHM, 10.-13.07.2018, Manchester, UK.
5. M. Scheerer, Z. Simon, M. Marischler, B. Rittenschober, „Influence of Production and Environmental Parameters on the behavior of hybrid Piezo / Temperature Sensors for Production and Structural Health Monitoring of Composite Structures”, Proc. of the 12th IWSHM, 10.-12.09.2023, Stanford, USA.
6. M. Scheerer, Z. Simon, M. Marischler, D. Kampenhuber, M. Hatzenbichler, “Validation of a piezo based integrated process and SHM system on hollow composite aircraft part made by vacuum infusion using a 3d printed smart mold”, Proc. of the 14th IWSHM, 11.-13.09.2023, Stanford, USA.
7. Ni Liu, Bin Ma, Feng Liu, Wenxuan Huang, Baosheng Xu, Lijie Qu, Yazheng Yang, “Progress in research on composite cryogenic propellant tank for large aerospace vehicles”, Composites Part A: Applied Science and Manufacturing, Volume 143, 2021, 106297.